Sensors & Actuators: B. Chemical 367 (2022) 132185

Contents lists available at ScienceDirect

Sensors and Actuators: B. Chemical

journal homepage: www.elsevier.com/locate/snb

Assembly of 2D-MoS_2 with graphene layer for highly sensitive and selective gas detection at room temperature

Xuemei Liu, Zehui He, Shiyuan Xu, Jiaying Wu, Jianmin Wu *

Lab of Nanomedicine and Omic-based Diagnostics, Institute of Analytical Chemistry, Department of Chemistry, Zhejiang University, Hangzhou 310058, PR China

ARTICLE INFO

Keywords:
Graphene oxide
Poly (diallyl dimethylammonium chloride)
Molybdenum disulfide
High sensitivity
Interlayer spacing
Gas sensor

ABSTRACT

Two-dimensional (2D) graphene has been regarded as a promising gas sensing material operated in room temperature. However, practical use of pure graphene as a gas sensor still faces problems owing to its insufficient sensitivity, selectivity and stability. In the present study, 2D-molybdenum disulfide (2D-MoS_2) were successfully assembled with graphene oxide (GO) with the assistance of poly (diallyl dimethylammonium chloride) (PDDA). The intercalation of PDDA and stacking of 2D-MoS_2 significantly expand the interlayer spacing of GO from 0.77 nm to 1.44 nm in the GO-PDDA-MoS_2 composite. The rGO-PDDA-MoS_2 sensing chip could be obtained by in-situ reduction of GO-PDDA-MoS_2 pre-coated on an interdigital electrode in hydrazine vapor. The sensor exhibited excellent sensitivity, selectivity and stability for H_2S and NO detection with a limit detection as low as 3 ppb and 5 ppb, respectively. The enhanced sensing performance could be ascribed to the increased gas accessibility and specific binding site resulted from the introduction of PDDA and 2D-MoS_2. Furthermore, its potential application in the diagnosis of respiratory disease was demonstrated. Exhaled breath (EB) spiked with 50 ppb NO and 15 ppb H_2S for simulating EB of asthma patients could be successfully discriminated from the normal EB.

1. Introduction

At present, the development of portable gas sensors with high sensitivity, high selectivity, fast response, and low-power consumption is still a challenge. Among many types of gas sensors, chemiresistive gas sensors are most likely to be used in practice because of their simple structure and excellent sensing performance [1,2]. However, most of chemiresistive gas sensors are developed from semiconductor metal oxides, which often need to operate at high temperatures [3,4], leading to higher power consumption and limits its application in Internet of Things (IoT) practice.

Graphene has unique advantages in gas-sensing field owing to its high specific surface area as well as high carrier mobility at room-temperature [5,6]. Among various formats of graphene nanomaterials for gas sensing, reduced graphene oxide (rGO) has been extensively used since it can be conveniently prepared by the reduction of graphene oxide (GO), which can be produced on a large scale at a relatively low cost. Unfortunately, pristine rGO has exhibited low sensitivity and selectivity probably due to its narrow band gap and lack of binding sites for specific gases. Meanwhile, the metastable oxygen containing functional groups on its surface lead to spontaneous reduction and stacking of layers [7], further resulting in low gas accessibility, decreased sensitivity and poor stability in gas detection.

Among various technologies, surface modification and synthesis of hybrid materials are the simplest ways to introduce specific binding sites and harness the band gap of graphene [8–10], thereby improving its stability and selectivity. For example, N-doped rGO was combined with PANI by hydrothermal synthesis, and a sensitive and selective response to 100 ppm NH_3 was observed [11]. By modifying rGO with In_2O_3, the nanosensor could successfully detect 50 ppm HCHO [12]. In our previous work, an E-Nose was constructed using metal-ion induced assembly of GO [13]. By introducing different metal ions, the composites displayed improved sensitivity and selectivity towards typical gases in exhaled breath. However, the sensitivity, selectivity and stability of current rGO-based chemiresistive sensors still need to be improved.

Transition metal dichalcogenides (TMDs), as a kind of metal-based materials, have been considered as promising nanomaterial in gas-sensing field due to their unique electrical, mechanical, and optical

Abbreviations: GO, graphene oxide; rGO, reduced graphene oxide; EB, exhaled breath; LOD, limit of detection; IDEs, interdigitated electrodes; ITO, indium tin oxide; PET, polyethylene terephthalate , LBL, Layer-by-layer.

* Corresponding author.
E-mail address: wjm-st1@zju.edu.cn (J. Wu).

https://doi.org/10.1016/j.snb.2022.132185
Received 6 April 2022; Received in revised form 5 June 2022; Accepted 6 June 2022
Available online 8 June 2022

properties [14,15]. Compared with other metal-based materials such as metal nanoparticles, metal oxides, and metal ions, TMDs have inherent advantages of 2D materials such as large specific surface area and more metal active sites [16,17]. Among TMDs, molybdenum disulfide (MoS_2) has aroused a great deal of interest in the past few years because of its unique electronic structure and suitable band gap [18–20]. However, the conductivity of pure MoS_2 is not enough to directly act as a chemiresistive sensor operated at room temperature. Combining MoS_2 with room temperature conductive graphene might be a good way to introduce sensitive and selective binding sites. Nevertheless, electrostatic repulsion between the same negatively charged MoS_2 and GO will hinder their binding and stacking [21]. Usually, the same charged nanomaterials can be assembled by layer-by-layer (LBL) self-assembly method with the assistance of polyelectrolytes. For example, poly (sodium-4-styrene sulfonate) (PSS) and poly (allylamine hydrochloride) (PAH) have been successfully employed to assemble negatively charged GO films by electrostatic force [22,23]. The positively charged TiO_2 was also assembled between PSS films as high sensitivity sensing material [24]. Typically, more than ten or even dozens of layers are generally required for LBL method, which lead to a quite complicated process and long operation time.

Herein, 2D-MoS_2, was successfully stacked with GO layer with the assistance of PDDA. As a positive charged long chain polymer, PDDA could insert between the negatively charged GO layers and assemble the 2D-MoS_2 with GO through electrostatic force, thereby promoting the formation of GO-PDDA-MoS_2 composite, as shown in Scheme 1(a). After deposition of GO-PDDA-MoS_2 on interdigital ITO-PET flexible electrode, the composite was in-situ reduced in hydrazine vapor, forming the rGO-PDDA-MoS_2 sensing chip. The rGO-PDDA-MoS_2 sensing chip exhibited excellent sensitivity, selectivity, and stability towards H_2S and NO at room temperature. The improved sensing performance may ascribe to the intercalation of PDDA and stacking of MoS_2, that may expand the interlayer spacing of GO/rGO and introduce abundant metal active sites. As the results, the gas accessibility and selective binding sites significantly increased. In the meanwhile, the stability of composite also greatly improved since the intercalated PDDA prevented rGO layers from re-stacking. To demonstrate its potential application in disease diagnosis, trace amount of H_2S and NO spiked in human exhaled breath (EB) was detected. The results indicated that the rGO-PDDA-MoS_2 gas sensor displayed a good quantitation ability. The present work will have promising application in the personal healthcare monitoring, especially in the preliminary screening of airway inflammation.

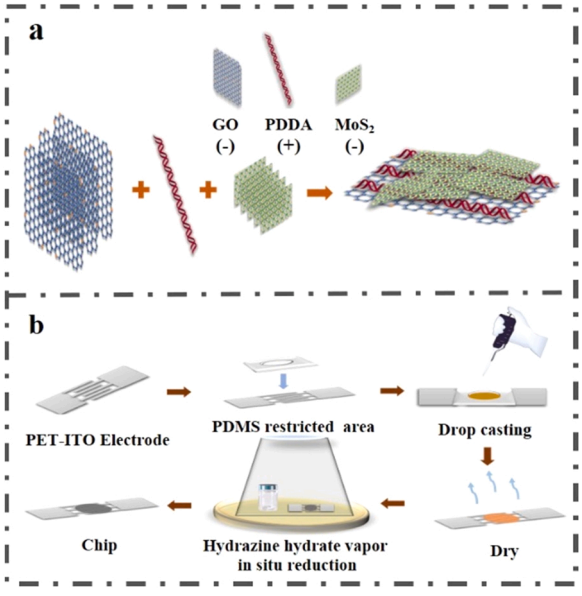

Scheme 1. (a) Schematic illustration for synthesis of GO-PDDA-MoS_2 composite; (b) Schematic diagram of the entire process for preparing sensing chip.

2. Materials and methods

2.1. Reagents and materials

PET film coated with ITO conductive layer (ITO-PET) was purchased from South China Science & Technology Co., Ltd (China). Photoresist S1805 (Shipley) for lithography was purchased from Anzhi lithography Electronic Materials Co., Ltd (Germany). Chemical reagents including HCl (36–38 %), HNO_3 (65–68 %), Acetone (≥99.5 %) and hydrazine hydrate (85 %) were purchased from Sinopharm Chemical Reagent Co., Ltd (China). Graphene Oxide (GO) sol was purchased from Chengdu Institute of Organic Chemistry, Chinese Academy of Science (CAS). Poly (diallyl dimethylammonium chloride) (PDDA, MW <10 kDa; MW =10–20 kDa; MW =20–35 kDa), poly (allylamine hydrochloride) (PAH, MW=30 kDa), Polyethyleneimine (PEI, MW =70KDa) and molybdenum disulfide (MoS_2) were purchased from Shanghai Macklin Biochemical Co., Ltd (China). Standard gases including H_2S (10 ppm in air), acetone (102 ppm in Air), NH_3 (202 ppm in N_2), NO (10.5 ppm in N_2), NO_2 (10 ppm in Air), isoprene (504 ppm in N_2), high purity CO_2, high purity air, and N_2 were purchased from Hangzhou Jingong Special Gas Co., Ltd, China.

2.2. Preparation of GO-PDDA and GO-PDDA-MoS_2

2D-MoS_2 was obtained by ultrasonic peeling method [21,25]. Briefly, 15 mg MoS_2 was added into 4 ml of 45 % ethanol aqueous solution and sonicated at 150 w for 2 h. The mixture was then centrifuged at 5000 rpm for 20 min. Finally, the supernatant was taken for later usage. The GO solution with a concentration of 0.5 mg/ml was also sonicated for 30 min before use.

GO-PDDA-MoS_2 composite was prepared by polymer mediated self-assembly method. Briefly, 15 μL (0.015 vol%) of PDDA (Mw. < 10 kDa, 1 %Wt) was added to the mixture of 0.5 ml GO and 0.5 ml MoS_2, and then the suspension was vibrated at room temperature on an oscillator for 5 h at 1000 rpm shaking rate. Then, the suspension was washed with deionized water 3 times to remove the free ions, excess GO, and MoS_2. Finally, the precipitation was redispersed in 1 ml deionized water. The GO-PDDA composite was prepared by the same method as mentioned above except that MoS_2 was not added. For comparison, GO-PAH and GO-PEI composites were also prepared by replacing PDDA with PAH and PEI, respectively.

2.3. Preparation of sensing chip

The IDEs of ITO-PET was fabricated by photolithographic methods as described in our previous work [26]. The entire process for preparing sensing chip is illustrated in Scheme 1(b). Firstly, a polydimethylsiloxane (PDMS) membrane with a hole was employed as a mask to restrict the sensing area. A droplet of 10 μL suspension containing the composite was loaded on the exposed area of ITO-PET IDEs. Then, the droplet was purged with N_2 stream and allowed to dry at room temperature. Finally, the chip was put into a chamber where hydrazine hydrate was heated to vapor at 70 °C and then the GO in the composite was reduced to rGO gradually. After 15 min, the sensing chip was taken out for later usage.

2.4. Materials characterization

The morphologies of GO, GO-PDDA, and GO-PDDA-MoS_2 were observed by scanning electron microscope (SEM) (Hitachi, SU8010, Japan). The elemental analysis was measured by X-ray photoelectron spectroscopy (XPS, VG ESCALAB MKII, UK) equipped with an Mg QR X-ray radiation source, and the interlayer spacing of composites was measured by diffraction of x-ray (XRD) (Bruker D8 Advance, USA).

Raman spectra were acquired by a Microscopic Raman spectrometer (Renishaw, 109907hk, UK) with a laser wavelength of 532 nm. Brunauer–Emmett–Teller (BET) surface area were performed on an gas adsorption analyzer (Micromeritics, Tristarll II 3020, USA). The sizes and thickness of 2D materials were investigated by atomic force microscope (AFM) (Bruker, Multi Mode 8, USA).

2.5. Measurement of gas sensor response

The concentration of gas sample was adjusted by mixing the standard gas and the carrier gas with an automatic gas distribution system (Well-Healthcare Technology Co., China), and then the gas was passed into a self-made chamber containing the gas sensing chip, which was operated at room temperature (25 °C). The bias voltage (typically 1.0 V) was applied by a power supply (KeySight E36103A, Keysight Technologies, Inc., USA). The current of the sensor was read out by a picoammeter (Keithley 6487, Keithley Instruments, Inc., USA) and the real-time current was recorded by LabVIEW 8.6 software. The measured current was then converted into resistance and the relative response signal (Re%) of the gas sensor is defined as follow equation:

$$Re\% = \frac{R - R_0}{R_0} \times 100 \quad (1)$$

Here, R_0 is the resistance in carrier gas stream, and R is the resistance measured in analytes exposure. The response/recovery time (t_{90}) is defined as the time to reach 90 % of the total resistance change.

2.6. Detection of H_2S and NO in exhale breath

In the EB analysis, a fluorinated ethylene propylene (FEP) bag was filled with 2 L healthy EB sample, which was collected in a room with good ventilation. Meanwhile, the atmospheric air was collected simultaneously in the same way as the carrier gas for EB analysis. Humidity influence in EB analysis can be avoided or alleviated by condensation method. Briefly, a Teflon tube was immersed in an ice-water bath to let sample gases flow through the tube. After such a treatment, the humidity of collected gases will decrease and keep the same (approximate to the saturated vapor pressure of H_2O at 0 °C).

The simulated EB samples of asthmatic patients were prepared by spiking standard NO and H_2S gas in EB samples collected from healthy persons. Briefly, 10 ml of 10.5 ppm NO and 3 ml of 10 ppm H_2S were injected into the FEP bag filled with healthy EB sample to reach final concentrations of 50 ppb and 15 ppb for NO and H_2S, respectively. As a control, an equal volume of N_2 was injected into another FEP bag filled with the same EB sample, and then the bags were rested at room temperature for 2 h to stabilize. During the testing process, the EB in the control bag and sample bag were sequentially pumped into the chamber installed with the gas sensor by a micro-pump with a flow rate of 200 sccm.

3. Results and discussion

3.1. Characterization of composite sensing materials coated on PET-ITO IDEs

To compare the homogeneity of films coated on ITO-PET IDEs, different types of sensing materials including GO, GO-PDDA, and GO-PDDA-MoS_2 were coated on the IDEs by dropping methods, respectively. After drying, the three types of sensing chips were exposed to hydrazine vapor, turning GO component to rGO. Each type of sensing film coated on the IDEs was observed with a reflectance microscopy. As we can see from Fig. S1a, the sensing film formed from GO solution was transparent but coffee-ring effect was observed. For the GO-PDDA film, aggregated particles were observed on the ITO-PET IDEs (Fig. S1b). In contrast, the film of GO-PDDA-MoS_2 appeared more homogeneous (Fig. S1c).

The morphologies of reduced composites were further investigated by SEM and TEM (Fig. 1a). As shown in the SEM images, the composites retained a layered structure of rGO (insert in Figs. 1a-1), but the layers were folded as viewed in a macroscopic structure. Compared with rGO, the rGO-PDDA and rGO-PDDA-MoS_2 films became more porous and wrinkled (Fig. 1a-1, a-2). The TEM image of rGO-PDDA showed randomly aggregated thin sheets with many wrinkles (Figs. 1a-3), whereas in rGO-PDDA-MoS_2 nanostructure, small MoS_2 sheets stacked on the rGO layer (1–2 μm) was found (Figs. 1a-4). XRD patterns of GO, GO-PDDA and GO-PDDA-MoS_2 before reduction in hydrazine vapor were shown in Fig. 1b-1. The GO presented a diffraction peak at 11.51°, which was consistent with the results previously reported [27–29]. For the GO-PDDA, the diffraction peak shifted toward a lower diffraction angle to 8.07°, indicating interlayer spacing of GO increased [30]. From the XRD pattern of GO-PDDA-MoS_2, the peak further shifted to 6.15°, reflecting that the interlayer spacing of GO further increased. According to the Bragg equation $2d\sin\theta = n\lambda$, the calculated interlayer spacing of GO, GO-PDDA, and GO-PDDA-MoS_2 were 0.77 nm, 1.09 nm, and 1.44 nm, respectively. In addition, a very weak diffraction peak appeared around 23° (Figs. 1b-1) owing to incomplete peeling of GO sheet that leads to the presence of graphite oxide residue. Besides, a weak diffraction peak appeared at 12.02° was observed in GO-PDDA--MoS_2 sample. The result had a slight difference compared with the previous reported peak value assigning to MoS_2 [31,32] due to the increase of MoS_2 interlayer spacing in the present work. The survey XPS spectra of GO indicated the existence of C, O element. However, the N1s peak was not observed in the survey spectra of GO-PDDA (Fig. 1b-2), probably owing to the low amount of PDDA in the composite (0.015 vol %). From the XPS spectra of GO-PDDA-MoS_2, a weak S2s peak and S2p peak were observed, while the Mo3d peak was not observed. Hence, it could be speculated that only a small amount MoS_2 stacked on GO due to the fact that MoS_2 is less negatively charged compared with GO [21]. For the high-resolution C1s spectrum, four fitted peaks located at 284.5 (C═C, C-C, C-H), 285.5(C-O-C), 287.5(C═O) and 288.4(O═C-O) [33, 34] could be observed in GO sample (Fig. 1c-1). In GO-PDDA-MoS_2, the characteristic peaks of GO could still be observed (Fig. 1c-2), confirming that GO retained in the composite. Compared with pure GO, the peaks for GO-PDDA-MoS_2 shifted to higher binding energy, reflecting a stronger interaction among PDDA, MoS_2, and GO in the composite. High-resolution XPS scans for GO-PDDA and GO-PDDA-MoS_2 showed the existence of N peak and Mo peak (Fig. 1c-3-c-4) [32,35], further suggesting that PDDA and MoS_2 were successfully combined with GO.

The AFM images of as-prepared rGO and MoS_2 nanosheets indicated that the lateral dimensions of rGO and MoS_2 were in the range of 1–2 μm and 200–400 nm with thickness of ~1–1.5 nm [36] and ~1.5–2 nm, respectively (Fig. 1d). According to the thickness of single layer rGO and 2D-MoS_2, the as-prepared rGO and MoS_2 nanosheets had a number of ~ 4 and 3 layers [36,37]. The structure of 2D materials were further characterized by Raman spectroscopy. For the GO and rGO, both D-band at ~1345 cm^{-1} and G-band at ~1590 cm^{-1} were observed (Fig. 1e-1). The D-band was ascribed to defects and disordered carbon, while the G-band represented the vibration of ordered sp^2-C in a 2D hexagonal lattice. Generally, the intensity ratio of the D and G could be employed to evaluate the degree of disorder and defect. The increased I_D/I_G value of rGO (1.128) compared to that of GO (0.916) indicated the higher degree of disordering and defects in the rGO structure. Furthermore, the sizes of crystalline domains in GO and rGO flakes can be estimated by I_D/I_G ratio and excitation wavelength of Raman spectrum as expressed by following equation [38,39]:

$$\mathrm{La(nm)} = \left(2.4\mathrm{x}10^{-10}\right) \quad \lambda_{laser}^4 \left(\frac{I_D}{I_G}\right)^{-1} \quad (2)$$

where La is the size of the crystalline domains in materials, λ_{laser} is the excitation wavelength of the Raman spectra. In the present work, the excitation wavelength was 532 nm, whereas the I_D/I_G values of GO and rGO were 0.916 and 1.128, respectively. Accordingly, crystalline

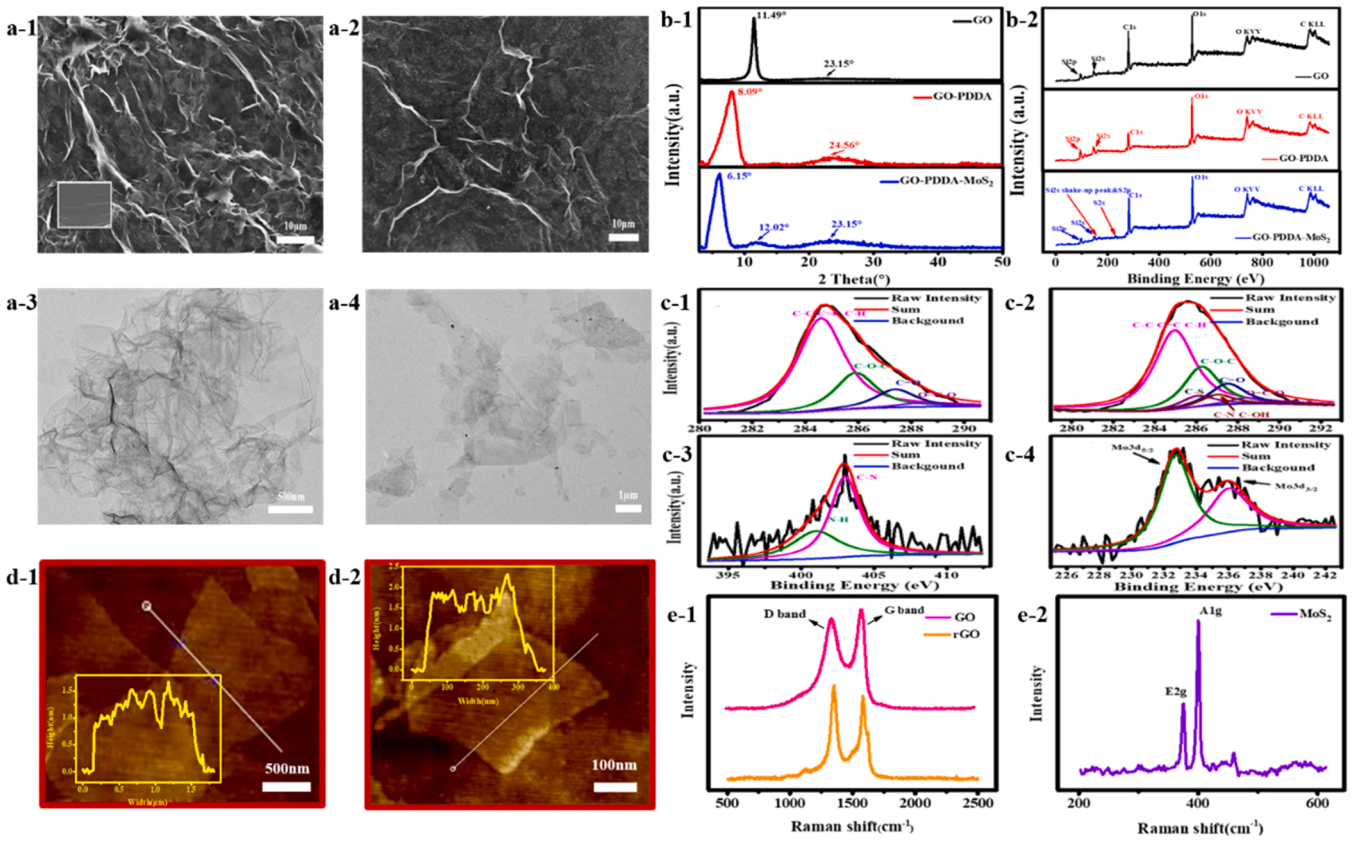

Fig. 1. SEM images of reduced composites. (a-1) rGO (insert in (a-1)) and rGO-PDDA; (a-2) rGO-PDDA-MoS_2; TEM images of reduced composites. (a-3) rGO-PDDA; (a-4) rGO-PDDA-MoS_2.; (b-1) XRD spectra and (b-2) XPS spectra of different materials. (c) High-resolution scan spectra and peak fitting results of different materials. C1s of (c-1) GO; (c-2) GO-PDDA-MoS_2; (c-3) N1s of GO-PDDA; (c-4) Mo3d of GO-PDDA-MoS_2. (d) AFM images of (d-1) rGO; (d-2) MoS_2. (e) Raman spectra of (e-1) GO and rGO; (e-2) MoS_2.

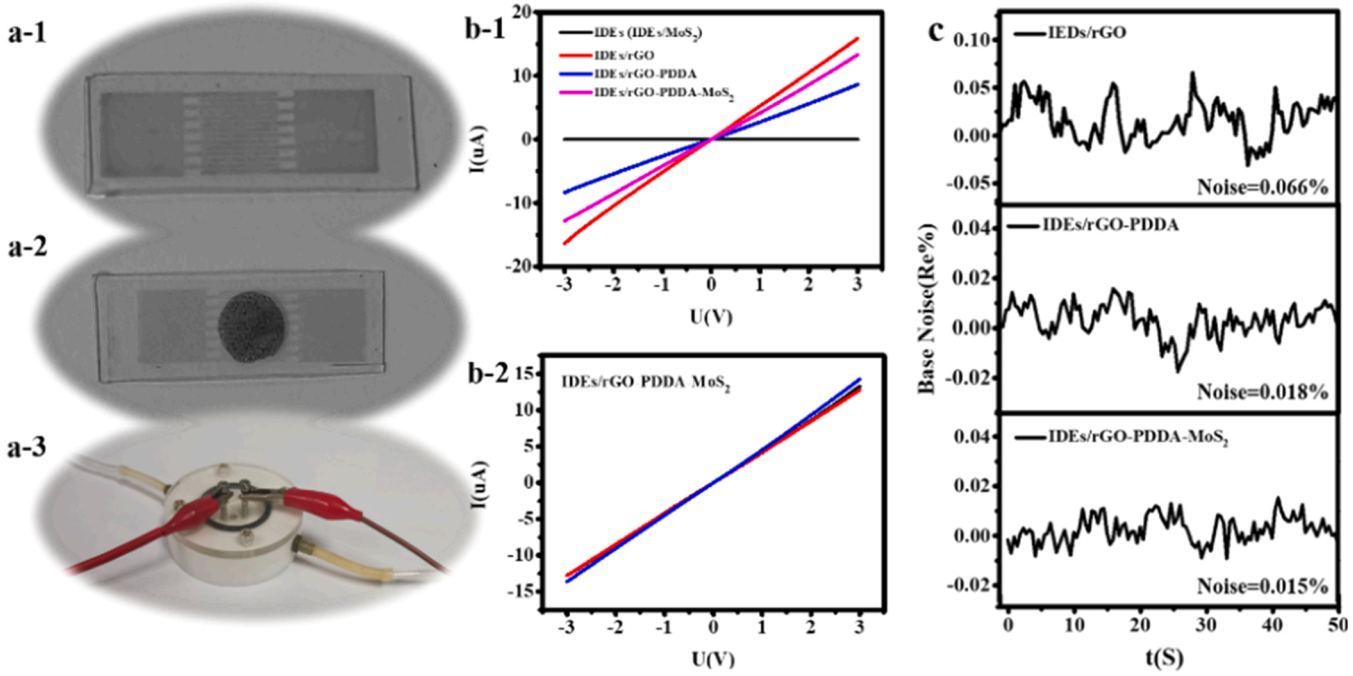

Fig. 2. The pictures of (a-1) ITO-PET IDEs; (a-2) ITO-PET IDEs after deposition of composite; (a-3) Laboratory self-made gas tank; I-V curves of (b-1) different materials on ITO-PET IDEs; (b-2) three times tests of rGO-PDDA-MoS_2 on ITO-PET IDEs; (c) The baseline noises of different materials on ITO-PET IDEs.

domains with the sizes at ca. 20.99 nm and 17.04 nm were formed in GO and rGO nanosheets, respectively. In the Raman spectrum of MoS_2, two characteristic peaks at 375.8 cm^{-1} and 401.1 cm^{-1} ascribing to the $E_{2\,g}$ and $A_{1\,g}$ mode of the MoS_2 were observed (Figs. 1e-2). Also, the number of MoS_2 layers was estimated to be ~3–4 according to the peak distance (25.3 cm^{-1} in this work) between the $E_{2\,g}$ and $A_{1\,g}$ vibration mode [40]. The results were consistent with the AFM results described above. Surface area and pore diameter of the materials were further investigated by BET analysis. The N_2 adsorption-desorption isotherm curves of rGO and rGO-PDDA-MoS_2 exhibited a type-IV isotherm (Fig. S2). The BET specific surface area of rGO-PDDA-MoS_2 nanocomposite was calculated to be 391.65 m^2/ g, which was about the twice of rGO nanosheets (258.67 m^2/g). The pore size distribution plots (inset of Fig. S2) illustrated that the main pore diameter of rGO-PDDA-MoS_2 (37 nm) was slightly smaller than that of rGO film (43 nm). The higher surface area and porous structure of nanocomposite could provide more binding sites for gas adsorption, making it an ideal candidate for gas sensing.

The device characteristics of sensing chips prepared from the three types of nanomaterials were measured by current-voltage (*I-V*) curves (Fig. 2a). As shown in Fig. 2b, stable and repeatable linear *I-V* curves were found in all types sensing chips, displaying an ohmic contact characteristics between the nanomaterials and ITO-PET IDEs. Meanwhile, electrical noises of rGO-PDDA and rGO-PDDA-MoS_2 sensing chips were lower than that of rGO chip (Fig. 2c), indicating that rGO-PDDA and rGO-PDDA-MoS_2 have a better electrode contact with ITO-PET IDEs.

3.2. Evaluating gas sensing performance of rGO-PDDA-MoS_2 prepared in different conditions

The negative charged GO could be assembled by positive charge polymers. Hence, the type of polymer was screened among PDDA, PAH, and PEI by measuring the response of rGO-PDDA, rGO-PAH, and rGO-PEI to 1 ppm H_2S. Among the three types of composites, the rGO-PDDA achieved the maximum response (Fig. 3a), probably owing to the existence of π-π stacking force between PDDA and GO. Meanwhile, sensing performance of composites derived from three types of 2D materials including MoS_2, WS_2, and hBN were evaluated. The result indicated that rGO-PDDA-MoS_2 displayed the highest response (Fig. 3b), showing the significant advantage of 2D-MoS_2 over WS_2, and hBN. In addition, the amount and molecular weight of PDDA were also optimized. The composite with PDDA content of 0.015 vol% and molecular weight < 10KDa achieved the best performance. Accordingly, it was selected as the sensing material for later usage (Fig. 3c-d).

3.3. Gas sensing performance of the optimized rGO-PDDA-MoS_2

The gas sensing performance of the rGO, rGO-PDDA, and optimized rGO-PDDA-MoS_2 sensing chips at room temperature were measured, respectively. (Fig. 4a~d). It was found that the rGO-PDDA-MoS_2 sensing chip has the largest resistance response when it was exposed to H_2S (Fig. 4a-c). The sensitivity of rGO-PDDA-MoS_2 to H_2S significantly increased and the value of Re% of rGO-PDDA-MoS_2 sensing chip to 1 ppm H_2S was nearly 14.5 times compared with that of pure rGO (Fig. 4d). As mentioned in Section 3.1, after adding PDDA and MoS_2, the interlayer spacing of GO increased from 0.77 nm to 1.44 nm, so that the gas accessibility in the nanostructured composites greatly improved. Meanwhile, the introduction of MoS_2 enhances the binding ability between H_2S and sensing material by producing more selective adsorption sites. All these factors contribute to the increase of sensitivity. The Re% of the three types of sensors towards five types of gases including H_2S, NO, NH_3, Acetone, and Isoprene were compared (Fig. 4e). The results showed that the resistance response to NO was second only to H_2S. The real-time relative response curves of the three types of sensing chips toward NO also indicated that the rGO-PDDA-MoS_2 sensing chip achieved the highest sensitivity towards NO (Fig. 4f). The improved sensitivity of rGO-PDDA-MoS_2 chip compared with that of rGO could be mainly ascribed to the increased gas accessibility. In order to prove the selectivity of rGO-PDDA-MoS_2 to H_2S, isoprene was selected as a reference and the ratio of response, Re (H_2S)/Re (Isoprene), obtained on the three types of sensors was calculated. The results indicated that the ratio of response at rGO-PDDA-MoS_2 significantly increased (Fig. 4g), indicating that the rGO-PDDA-MoS_2 sensing chip had good selectivity to H_2S. Furthermore, the rGO-PDDA-MoS_2 sensing chip also displayed a good repeatability to 200 ppb H_2S (Fig. 4h) with a response/recovery time (t_{90}) of 34 s and 50 s, respectively (Fig. 4i). The initial response within 10 s could also indicated the response kinetics of different

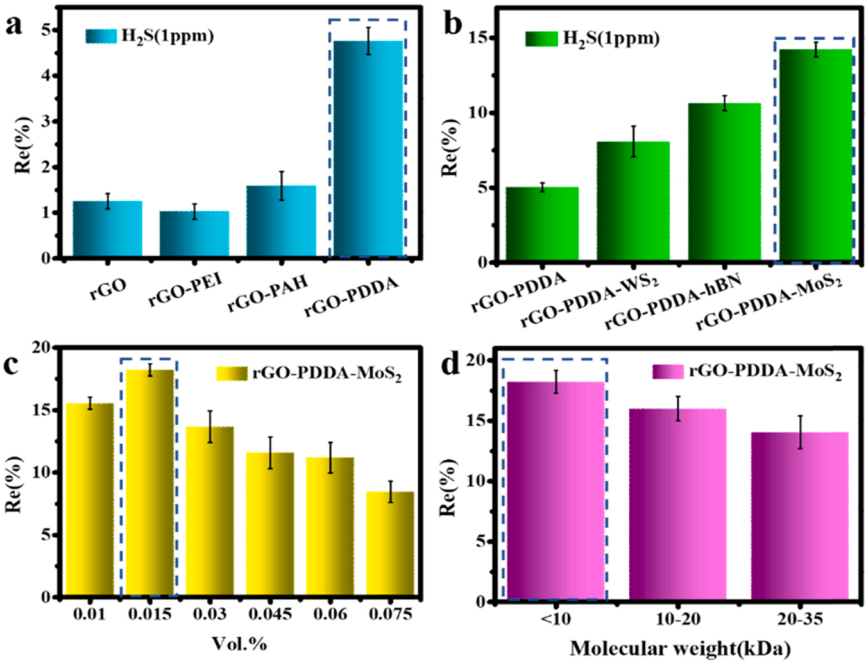

Fig. 3. Re% of sensing chips to 1 ppm H_2S at (a) different polycation electrolytes; (b) different 2D materials; Re% of rGO-PDDA-MoS_2 sensing chip to 1 ppm H_2S at (c) different amounts and (d) different molecular weights of PDDA.

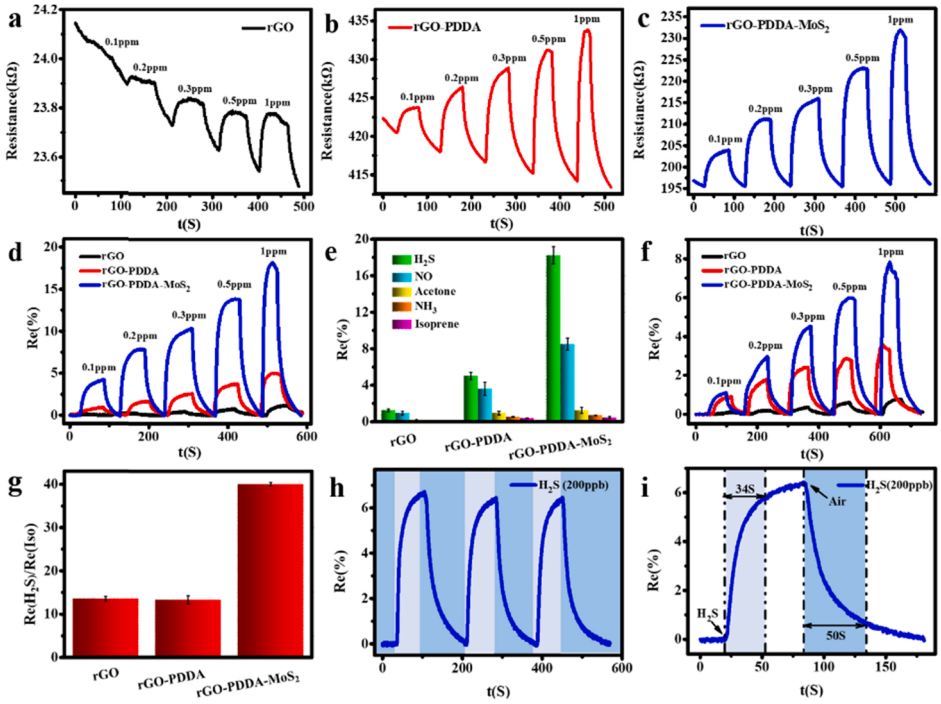

Fig. 4. The real-time resistance response of (a) rGO (b) rGO-PDDA (c) rGO-PDDA-MoS_2 sensing chips toward H_2S; (d) The comparison of real-time relative resistance response between rGO; rGO-PDDA; rGO-PDDA-MoS_2 sensing chips toward H_2S; (e) The relative resistance response obtained on three types of sensing chips to H_2S, NO, NH_3, Acetone, and Isoprene (All of them were 1 ppm except Isoprene was 2 ppm); (f) The comparison of real-time relative resistance response between rGO; rGO-PDDA; rGO-PDDA-MoS_2 sensing chips toward NO; (g) The comparison of Re(H_2S)/Re (Isoprene) ratio among rGO; rGO-PDDA; rGO-PDDA-MoS_2 sensing chips; (h) Response repeatability and (i) response/recovery time of rGO-PDDA-MoS_2 sensing chip to 200 ppb H_2S.

sensors. According to the sensing curves shown in Fig. 4d, the initial responses of rGO, rGO-PDDA and rGO-PDDA-MoS_2 were 0.004, 0.024 and 0.233, respectively. The remarkable quicker response on rGO-PDDA-MoS_2 compared to that on other types of sensors could be also ascribed to the expanded interlayer spacing, which facilitate gas diffusion and circulation. Besides, the response signal toward H_2S and NO at sub-ppm concentration was further analyzed, and the Re% could be fitted with the Langmuir model well (Fig. S3). At low concentrations, a good linear relationship was found between the Re% and concentration (Fig. S4). The linear regression equations of rGO-PDDA-MoS_2 sensor for H_2S and NO were $Re\% = 31.7c\text{-}0.14$ and $Re\% = 20.6c\text{-}0.65$, where c is the concentration of H_2S or NO, respectively. The theoretical LOD of rGO-PDDA-MoS_2 sensing chip for H_2S and NO can reach as low as 3 ppb and 5 ppb, respectively (6δ/S), suggesting huge advantages compared with other H_2S sensors reported previously (Table S1).

The resistance response of rGO-PDDA-MoS_2 sensing chip towards another nitric oxide, NO_2, was also measured. The sensing chip displayed an upward resistance signal and the Re (%) to 1 ppm NO_2 was ~6.33 % (Fig.S5a), which was slightly lower than that of NO (8.14 %). In the range of 0.1–1.0 ppm, the relationship between Re% and gas concentrations could be also fitted well with the Langmuir model (Fig. S5b). Even though, the sensor displays sensitive response to NO_2, the interference can be negligible in the analysis of human exhaled breath (EB) gas, since the concentration of NO_2 is far less than that of NO in EB sample. Concerning the high amount of CO_2 in human EB, the response of rGO-PDDA-MoS_2 sensing chip towards CO_2 was also evaluated. As we can see from the sensor diagram, the response value to 0.25 % (2500 ppm) CO_2 was only 0.24 % (Fig. S6a), showing much low response to CO_2 compared with other target gases. PDDA polymer in the sensing materials contains abundant NH_2 groups, which should have affinity to CO_2 owing to the acid-base interaction. The low sensitivity toward CO_2 gas might be ascribed to the inert chemical property of CO_2, such as non-polarity and low capability of electron transfer. In the concentration range from 0.25 % to 3.0 %, linear relationship was found between the Re% and CO_2 concentration (Fig. S6b). As observed in the linear curve, high concentration of CO_2 will also produce significant response. For the human EB detection, the response caused by CO_2 could be regarded as a background signal, which could be subtracted in data pretreatment. The detail method will be discussed in Section 3.6. In order to further study whether exposure to CO_2 will deteriorate the sensing performance, we measured the response dynamic curves of the sensing chip to H_2S and NO after being exposure to pure CO_2 for 30 min. The results showed that the sensing chip still had high sensitivity and good response/recovery ability to H_2S and NO (Figs. S6c-d), indicating that the exposure of CO_2 would not deteriorate the sensing performance of rGO-PDDA-MoS_2 sensing chip.

3.4. *Stability and humidity influence of the rGO-PDDA-MoS_2 sensing chip*

Short-term and long-term stabilities of the sensing chip were explored, respectively. Compared with rGO, the rGO-PDDA-MoS_2 sensor chip displayed better stability within 7 days at room temperature (Fig. 5a). In addition, the long-term stability of the sensor was investigated with high temperature accelerated experiment. The rGO-PDDA-MoS_2 sensing chip was placed in an oven at 55 °C. The response signal to 1 ppm H_2S during 8 days was measured and the response decay (Re/Re_0) could be calculated (Fig. S7). According to the Arrhenius equation, the activation energy (Ea) for aging process on rGO-PDDA-MoS_2 is around 1.09ev. Therefore, we could estimate that the life time of the sensor will up to 1.5 years at room temperature. Meanwhile, the response repeatability and response/recovery time of the aged sensing chip to 200 ppb H_2S were tested. The results showed that the aged sensing chip still retained high sensing performance (Fig. S8). It is well known that the metastable oxygen containing functional groups on the surface of rGO will lead to spontaneous reduction and re-stacking of 2D material [7], which causes a loss of the sensitivity of gas detection and further results in poor stability. In the present study, the introduction of PDDA and MoS_2 to the interlayer of rGO may prevent rGO from re-stacking. Therefore, its stability was significantly improved.

Furthermore, the humidity influence of the rGO-PDDA-MoS_2 sensing chip at room temperature was studied. As we can see from Fig. 5b, with the increase of relative humidity, the relative response of rGO-PDDA-MoS_2 sensing chip toward H_2S decreased. However, the decrease of the response value can be calibrated by relative humidity as shown in Fig. 5c. Thus, we can equip the device with a moisture sensor and correct the response value if divided the measured response value by the

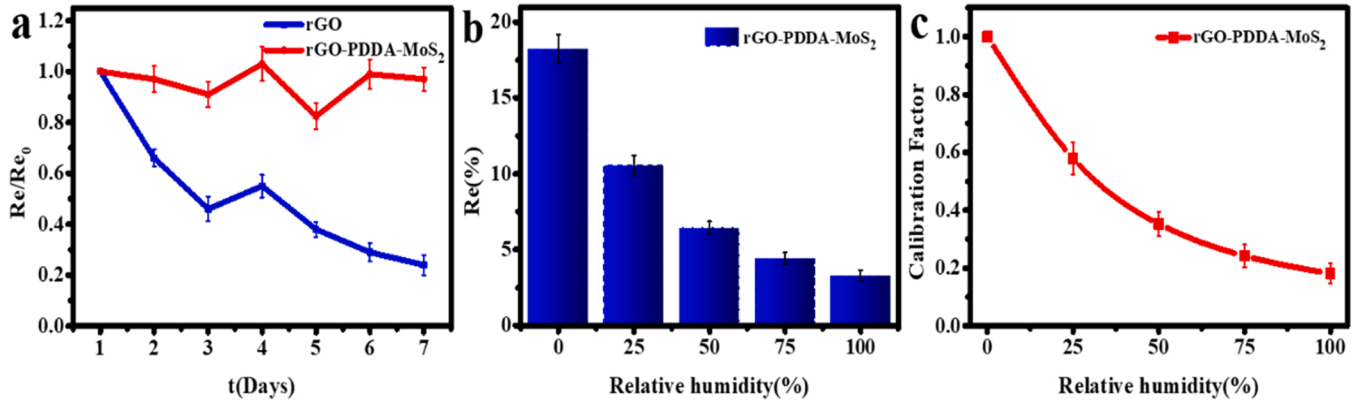

Fig. 5. (a) Response decay of rGO and rGO-PDDA-MoS_2 sensing chips to 1 ppm H_2S within 7 days at room temperature. Re is the relative response of sensor at different time, whereas Re_0 is the initial relative response of the sensor. (b) Re% of the rGO-PDDA-MoS_2 sensing chip at different relative humidity. (c) Humidity calibration factor for the rGO-PDDA-MoS_2 sensing chip, (Humidity calibration factor = Re% (H%)/Re% (0%)). The relative humidity was adjusted by different saturated salt solutions.

humidity calibration factor.

3.5. Mechanism study

rGO has been regarded as a p-type semiconductor owing to the oxygen functional groups located on its surface. The introduction of reduced gases will lead to a decrease of the majority carrier (holes) and thereby increasing resistance of sensing element, further resulting in an upward response (Fig. 4a-d). After adding PDDA, the rGO-PDDA composite showed much higher sensitivity to each gas (Fig. 4e) than that of rGO. We attribute the enhanced sensing property of rGO-PDDA to the following three aspects.

First, GO is a negatively charged 2D material due to oxygen-containing functional groups located on the surface, while PDDA is a typical positively charged polycation electrolyte. Consequently, the PDDA will insert between the GO nanosheets through electrostatic attracting force, leading to the expansion of interlayer spacing (increase from 0.77 to 1.09 nm as mentioned in Section 3.1), which is crucial in contributing to the high sensitivity. The wider interlayer spacing offers a much larger exposed surface to target analytes and significantly improves gas accessibility, as illustrated in Fig. 6a-b. Second, the swollen effect can also influence the sensitivity toward gases. The mechanism proposed by Neugebauer and Webb could be expressed as following formulas [41–43].

$$\sigma \propto e^{-2\delta\beta} e^{-Ec/kT} \quad (3)$$

$$Ec \approx e^2/(4\pi\varepsilon_r\varepsilon_0 r) \quad (4)$$

where σ is the conductivity of the composite, representing the ability of electrons crossing; δ is the interlayer spacing; β is the quantum mechanical tunneling factor; Ec is the activation energy; ε_r and ε_0 are the permittivities, and r is the radius of a nanocluster. When the sensing material was exposed to different gases, the analytes will adsorb on the active sites, forming π-complex or σ-complex [13], leading to an increase of δ and decrease of σ. The intercalation of PDDA makes the swollen effect more significant, thus further resulting in improved sensing sensitivity. Third, the porous structure and morphology can also contribute to the improved sensitivity. As we can see in Fig. 1a, compared with rGO, rGO-PDDA film has porous and wrinkled nanostructures, which facilitate the gas diffusion and adsorption.

After the stacking of MoS_2 on rGO nanosheets with the assistance of PDDA as illustrated in Fig. 6c, the layer spacing increase to 1.44 nm (as mentioned in Section 3.1), thereby further enhancing the gas accessibility and improving sensitivity (Fig. 4d). Meanwhile, the introduction of MoS_2 produces more selective adsorption sites and enhance the binding ability between H_2S and the sensing material, resulting in the

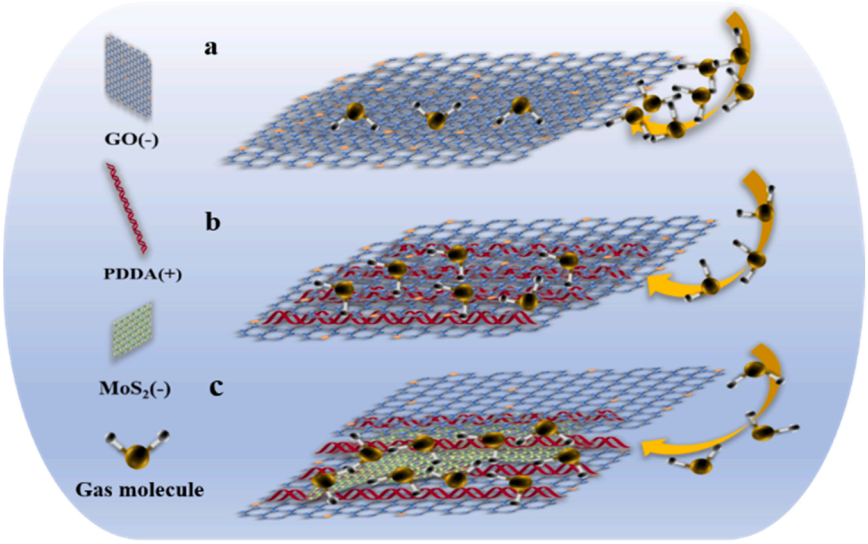

Fig. 6. Schematic diagram of the mechanism of (a) rGO; (b) rGO-PDDA; (c) rGO-PDDA-MoS_2.

largest sensing selective to H_2S as we can see in Fig. 4e.

3.6. Measurements of H_2S and NO on EB simulating asthma patients

Asthma, a chronic inflammatory disease of the airway, is characterized by paroxysmal and reversible airflow obstruction [44]. It is the most common chronic disease of childhood and affects 1 %− 18 % of the population in different countries [45]. However, the ability to diagnose children at high risk for persistent asthma remains limited [46]. It has been reported that H_2S and NO are two typical EB markers in asthmatic patients. The levels of H_2S in EB of asthmatic patients can reach 15.7 ppb [47]. Another study reported an average of 44 ppb NO in the EB of asthmatic patients [48]. As a proof-of-concept work, the potential of the rGO-PDDA-MoS_2 sensing chip for the primary asthma diagnosis was evaluated. The experimental setup and procedure were illustrated in Fig. 7a-b. The response signal of rGO-PDDA-MoS_2 sensor to simulated EB of asthma patients and EB of healthy people were measured, respectively. After 10 cases of study, it can be seen from the box chart that the relative resistance response (Re%) of simulated EB of asthma patients was much higher than that of healthy people (Fig. 7c). As we mentioned in Section 3.3, compared with other target gases, the sensing chip had low sensitivity to CO_2, nevertheless, the concentration of CO_2 in EB is ~4 %, which will still produce a significant response in EB detection. However, the response signal caused by CO_2 will not affect the EB classification between healthy and asthma patients, as the concentrations of CO_2 are almost the same among individuals. In disease classification, the signal caused by CO_2 could be regarded as a part of background signal, and the increments of signal in asthma patients compared to healthy could be act as the disease indicator. To further confirm that the difference in response signals of healthy and asthma patients were generated by the added standard gases, the response of simulated EB of asthma patients was measured when the EB of healthy people was used as the blank gas. In this detection, the signal caused by CO_2 and other background gas components in human EB could be subtracted. As illustrated in Fig. 7d, a remarkable response signal could still be observed on the rGO-PDDA-MoS_2 sensor. According to the linear regression equation of rGO-PDDA-MoS_2 sensor, the sum of theoretical response value produced by spiked 15 ppb H_2S and 50 ppb NO is about 0.75, which is almost consistent with the measured Re% of 0.72 ± 0.03 ($n = 10$, $P = 0.95$) (Fig. 7d), indicating that the sensor has a good quantitative ability.

4. Conclusion

In summary, we demonstrated that the sensing chip prepared by stacking 2D-MoS_2 on rGO nanosheets with the assistance of PDDA could act as a promising active material to enhance the gas sensing sensitivity at room temperature. The sensing chip displayed higher sensitivity and selectivity towards H_2S and NO, which are two important biomarkers for airway inflammation. The theoretical LOD for H_2S and NO can reach as low as 3 ppb and 5 ppb, respectively. Compared with rGO, the rGO-PDDA-MoS_2 sensing chip shows good repeatability and fast response/recovery speed, as well as better short-term and long-term stability. Furthermore, the mechanism for explaining the high sensitivity, selectivity and stability of rGO-PDDA-MoS_2 sensing chip was investigated. Owing to the insertion of PDDA, the interlayer spacing of GO increased. After introducing MoS_2, it stacks on GO with the assistance of PDDA, and the interlayer spacing of GO further expands. The larger interlayer spacing offers higher exposed surface area and improved gas accessibility, which is crucial in contributing to the high sensitivity. Meanwhile, the existence of PDDA prevents the re-stacking of rGO and enhances the swollen effect between the rGO layer, leading to improved stability and sensitivity for gas detection. Besides, MoS_2 produces more selective adsorption sites and enhances the binding ability between H_2S and sensing material, causing the selective response towards H_2S. As a proof-of-concept application in disease diagnosis, simulated EB of asthma patients was prepared and tested. The response signal was almost consistent with the theoretical response corresponding to the

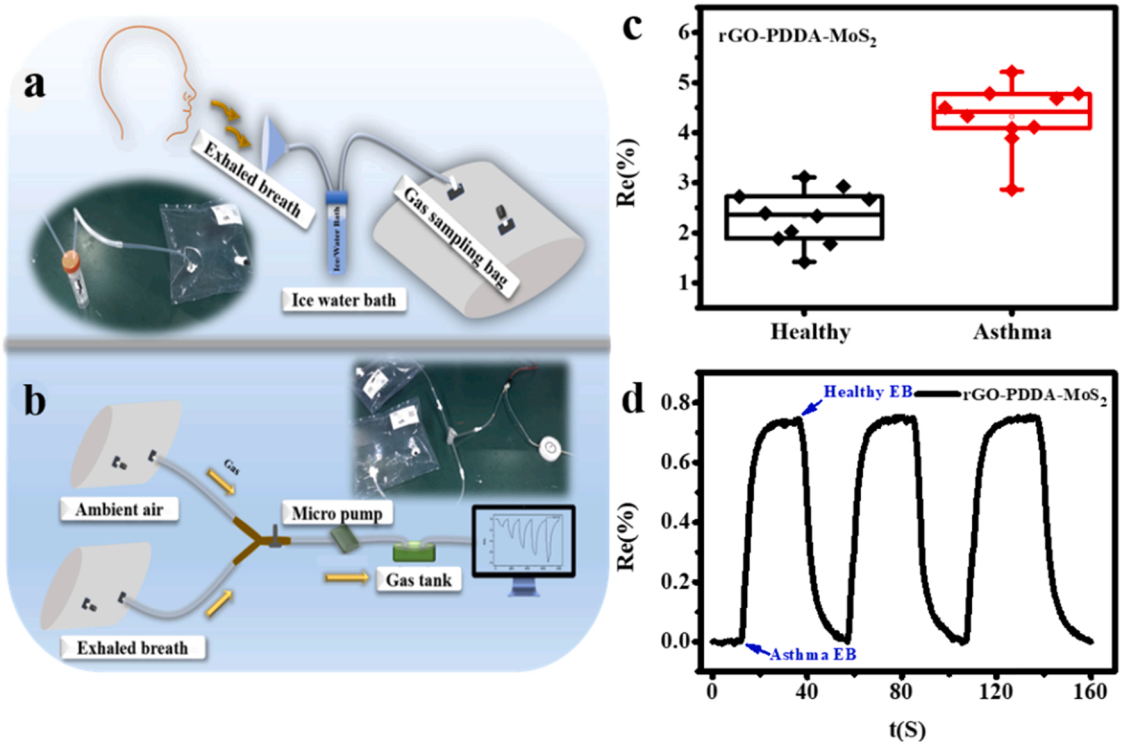

Fig. 7. Experimental setup and senor response for EB detection. (a) EB sampling method; (b) Experimental setup for EB detection, in which the ambient air was used as the blank gas; (c) Box chart of sensor response generated by healthy EB and simulated asthma EB; (d) Real-time sensor response towards simulated asthma EB when the healthy EB act as the blank gas.

spiked concentration of NO and H_2S, showing a good quantitation ability of the sensor. The present work will find promising applications in the field of personal healthcare monitoring, especially in the preliminary screening of airway inflammation.

CRediT authorship contribution statement

Xuemei Liu: Conceptualization, Validation, Formal analysis, Investigation, Resources, Writing – original draft. **Zehui He**: Data Curation, Writing – review & editing, Supervision. **Shiyuan Xu**: Writing – review & editing, Visualization, Supervision. **Jiaying Wu**: Project administration, Supervision. **Jianmin Wu:** Conceptualization, Resources, Supervision, Funding acquisition.

Declaration of Competing Interest

The authors declare that they have no known competing financial interests or personal relationships that could have appeared to influence the work reported in this paper.

Acknowledgements

This work was supported by National Natural Science Foundation of China (No. 21 575 127 and No. 21 874 118), and Zhejiang Provincial Key Research and Development Program (No. 2021C03124).

Appendix A. Supporting information

Supplementary data associated with this article can be found in the online version at doi:10.1016/j.snb.2022.132185.

References

[1] F. Schedin, A.K. Geim, S.V. Morozov, E.W. Hill, P. Blake, M.I. Katsnelson, et al., Detection of individual gas molecules adsorbed on graphene, Nat. Mater. 6 (2007) 652–655, https://doi.org/10.1038/nmat1967.
[2] J.D. Fowler, M.J. Allen, V.C. Tung, Y. Yang, R.B. Kaner, B.H. Weiller, Practical chemical sensors from chemically derived graphene, ACS Nano 3 (2009) 301–306, https://doi.org/10.1021/nn800593m.
[3] R. Kalidoss, S. Umapathy, R. Anandan, V. Ganesh, Y. Sivalingam, Comparative study on the preparation and gas sensing properties of reduced graphene Oxide/SnO_2 binary nanocomposite for detection of acetone in exhaled breath, Anal. Chem. 91 (2019) 5116–5124, https://doi.org/10.1021/acs.analchem.8b05670.
[4] H.Y. Li, Z.X. Cai, J.C. Ding, X. Guo, Gigantically enhanced NO sensing properties of WO_3/SnO_2 double layer sensors with Pd decoration, Sens. Actuators B: Chem. 220 (2015) 398–405, https://doi.org/10.1016/j.snb.2015.05.091.
[5] A. Peigney, C. Laurent, E. Flahaut, R.R. Bacsa, A. Rousset, Specific surface area of carbon nanotubes and bundles of carbon nanotubes, Carbon 39 (2001) 507–514, https://doi.org/10.1016/s0008-6223(00)00155-x.
[6] S. Drieschner, M. Weber, J. Wohlketzetter, J. Vieten, E. Makrygiannis, B. M. Blaschke, et al., High surface area graphene foams by chemical vapor deposition, 2D Mater. 3 (2016), https://doi.org/10.1088/2053-1583/3/4/045013.
[7] S. Kim, S. Zhou, Y. Hu, M. Acik, Y.J. Chabal, C. Berger, et al., Room-temperature metastability of multilayer graphene oxide films, Nat. Mater. 11 (2012) 544–549, https://doi.org/10.1038/NMAT3316.
[8] C. Wang, Y. Wang, Z. Yang, N. Hu, Review of recent progress on graphene-based composite gas sensors, Ceram. Int. 47 (2021) 16367–16384, https://doi.org/10.1016/j.ceramint.2021.02.144.
[9] Z. Chen, J. Wang, Y. Wang, Strategies for the performance enhancement of graphene-based gas sensors: a review, Talanta 235 (2021), 122745, https://doi.org/10.1016/j.talanta.2021.122745.
[10] T. Wang, D. Huang, Z. Yang, S. Xu, G. He, X. Li, et al., A review on graphene-based gas/vapor sensors with unique properties and potential applications, Nanomicro Lett. 8 (2016) 95–119, https://doi.org/10.1007/s40820-015-0073-1.
[11] N.R. Tanguy, M. Arjmand, N. Yan, Nanocomposite of nitrogen-doped graphene/polyaniline for enhanced ammonia gas detection, Adv. Mater. Interfaces (2019), https://doi.org/10.1002/admi.201900552.
[12] J.H. Choi, J.S. Seo, H.E. Jeong, K. Song, S.-H. Baeck, S.E. Shim, et al., Effects of field-effect and schottky heterostructure on p-type graphene-based gas sensor modified by n-Type In_2O_3 and phenylenediamine, Appl. Surf. Sci. 578 (2022), https://doi.org/10.1016/j.apsusc.2021.152025.
[13] Q. Chen, Z. Chen, D. Liu, Z. He, J. Wu, Constructing an E-Nose using metal-ion-induced assembly of graphene oxide for diagnosis of lung cancer via exhaled breath, ACS Appl. Mater. Interfaces 12 (2020) 17713–17724, https://doi.org/10.1021/acsami.0c00720.
[14] D. Sarkar, X. Xie, J. Kang, H. Zhang, W. Liu, J. Navarrete, et al., Functionalization of transition metal dichalcogenides with metallic nanoparticles: implications for doping and gas-sensing, Nano Lett. 15 (2015) 2852–2862, https://doi.org/10.1021/nl504454u.
[15] B.L. Li, J. Wang, H.L. Zou, S. Garaj, C.T. Lim, J. Xie, et al., Low-dimensional transition metal dichalcogenide nanostructures based sensors, Adv. Funct. Mater. 26 (2016) 7034–7056, https://doi.org/10.1002/adfm.201602136.
[16] W.Y. Chen, X. Jiang, S.N. Lai, D. Peroulis, L. Stanciu, Nanohybrids of a MXene and transition metal dichalcogenide for selective detection of volatile organic compounds, Nat. Commun. 11 (2020) 1302, https://doi.org/10.1038/s41467-020-15092-4.
[17] M. Donarelli, L. Ottaviano, 2D Materials for gas sensing applications: a review on graphene oxide, MoS_2, WS_2 and phosphorene, Sensors (2018), https://doi.org/10.3390/s18113638.
[18] X. Hou, Z. Wang, G. Fan, H. Ji, S. Yi, T. Li, et al., Hierarchical three-dimensional MoS_2/GO hybrid nanostructures for triethylamine-sensing applications with high sensitivity and selectivity, Sens. Actuators B: Chem. 317 (2020), https://doi.org/10.1016/j.snb.2020.128236.
[19] A.V. Agrawal, N. Kumar, M. Kumar, Strategy and future prospects to develop room-temperature-recoverable NO_2 gas sensor based on two-dimensional molybdenum disulfide, Nanomicro Lett. 13 (2021) 38, https://doi.org/10.1007/s40820-020-00558-3.
[20] A. Hermawan, N.L.W. Septiani, A. Taufik, B. Yuliarto, Suyatman, S. Yin, Advanced strategies to improve performances of molybdenum-based gas sensors, Nanomicro Lett. 13 (2021) 207, https://doi.org/10.1007/s40820-021-00724-1.
[21] K.G. Zhou, N.N. Mao, H.X. Wang, Y. Peng, H.L. Zhang, A mixed-solvent strategy for efficient exfoliation of inorganic graphene analogues, Angew. Chem. Int. Ed. Engl. 50 (2011) 10839–10842, https://doi.org/10.1002/anie.201105364.
[22] P.G. Su, Z.H. Liao, Fabrication of a flexible single-yarn NH_3 gas sensor by layer-by-layer self-assembly of graphene oxide, Mater. Chem. Phys. 224 (2019) 349–356, https://doi.org/10.1016/j.matchemphys.2018.12.043.
[23] Z. Yang, Y. Chen, J. Deng, Polyelectrolytes/reduced graphene oxide assembled film as a promising NO2 gas sensing material, Ceram. Int. 46 (2020) 5119–5125, https://doi.org/10.1016/j.ceramint.2019.10.255.
[24] D. Zhang, J. Liu, C. Jiang, P. Li, Ye Sun, High-performance sulfur dioxide sensing properties of layer-by-layer self-assembled titania-modified graphene hybrid nanocomposite, Sens. Actuators B: Chem. 245 (2017) 560–567, https://doi.org/10.1016/j.snb.2017.01.200.
[25] J.N. Coleman, M. Lotya, A. O'Neill, S.D. Bergin, P.J. King, U. Khan, et al., Two-dimensional nanosheets produced by liquid exfoliation of layered materials, Science 331 (2011) 568–571, https://doi.org/10.1126/science.1194975.
[26] Q. Chen, D. Liu, L. Lin, J. Wu, Bridging interdigitated electrodes by electrochemical-assisted deposition of graphene oxide for constructing flexible gas sensor, Sens. Actuators B: Chem. 286 (2019) 591–599, https://doi.org/10.1016/j.snb.2019.02.024.
[27] T. Kuila, S. Bose, A.K. Mishra, P. Khanra, N.H. Kim, J.H. Lee, Chemical functionalization of graphene and its applications, Prog. Mater. Sci. 57 (2012) 1061–1105, https://doi.org/10.1016/j.pmatsci.2012.03.002.
[28] H.J. Shin, K.K. Kim, A. Benayad, S.M. Yoon, H.K. Park, I.S. Jung, et al., Efficient reduction of graphite oxide by sodium borohydride and its effect on electrical conductance, Adv. Funct. Mater. 19 (2009) 1987–1992, https://doi.org/10.1002/adfm.200900167.
[29] C. Zhu, P. Wang, L. Wang, L. Han, S. Dong, Facile synthesis of two-dimensional graphene/SnO_2 /Pt ternary hybrid nanomaterials and their catalytic properties, Nanoscale 3 (2011) 4376–4382, https://doi.org/10.1039/c1nr10634a.
[30] A. Chen, R. Liu, X. Peng, Q. Chen, J. Wu, 2D hybrid nanomaterials for selective detection of NO_2 and SO_2 Using "Light On and Off" strategy, ACS Appl. Mater. Interfaces 9 (2017) 37191–37200, https://doi.org/10.1021/acsami.7b11244.
[31] M. Ikram, L. Liu, Y. Liu, L. Ma, H. Lv, M. Ullah, et al., Fabrication and characterization of a high-surface area MoS_2@WS_2 heterojunction for the ultra-sensitive NO_2 detection at room temperature, J. Mater. Chem. A 7 (2019) 14602–14612, https://doi.org/10.1039/c9ta03452h.
[32] Y. Jing, E.O. Ortiz-Quiles, C.R. Cabrera, Z. Chen, Z. Zhou, Layer-by-layer hybrids of MoS_2 and reduced graphene oxide for lithium ion batteries, Electrochim. Acta 147 (2014) 392–400, https://doi.org/10.1016/j.electacta.2014.09.132.
[33] S. Stankovich, D.A. Dikin, R.D. Piner, K.A. Kohlhaas, A. Kleinhammes, Y. Jia, et al., Synthesis of graphene-based nanosheets via chemical reduction of exfoliated graphite oxide, Carbon 45 (2007) 1558–1565, https://doi.org/10.1016/j.carbon.2007.02.034.
[34] P.G. Ren, D.X. Yan, X. Ji, T. Chen, Z.M. Li, Temperature dependence of graphene oxide reduced by hydrazine hydrate, Nanotechnology 22 (2011), 055705, https://doi.org/10.1088/0957-4484/22/5/055705.
[35] C. Xu, Rs Yuan, X. Wang, Selective reduction of graphene oxide, N. Carbon Mater. 29 (2014) 61–66, https://doi.org/10.1016/S1872-5805(14)60126-8.
[36] K.K.H. De Silva, P. Viswanath, V.K. Rao, S. Suzuki, M. Yoshimura, New insight into the characterization of graphene oxide and reduced graphene oxide monolayer flakes on si-based substrates by optical microscopy and raman spectroscopy, J. Phys. Chem. C. 125 (2021) 7791–7798, https://doi.org/10.1021/acs.jpcc.1c01152.
[37] J. Zhu, H. Xu, G. Zou, W. Zhang, R. Chai, J. Choi, et al., MoS_2-OH bilayer-mediated growth of inch-sized monolayer MoS_2 on arbitrary substrates, J. Am. Chem. Soc. 141 (2019) 5392–5401, https://doi.org/10.1021/jacs.9b00047.
[38] M.A. Pimenta, G. Dresselhaus, M.S. Dresselhaus, L.G. Cancado, A. Jorio, R. Saito, Studying disorder in graphite-based systems by Raman spectroscopy, Phys. Chem. Chem. Phys. 9 (2007) 1276–1291, https://doi.org/10.1039/b613962k.

[39] N. Hu, Y. Wang, J. Chai, R. Gao, Z. Yang, E.S.-W. Kong, et al., Gas sensor based on p-phenylenediamine reduced graphene oxide, Sens. Actuators B: Chem. 163 (2012) 107–114, https://doi.org/10.1016/j.snb.2012.01.016.
[40] A.S. George, Z. Mutlu, R. Ionescu, R.J. Wu, J.S. Jeong, H.H. Bay, et al., Wafer scale synthesis and high resolution structural characterization of atomically thin MoS_2 Layers, Adv. Funct. Mater. 24 (2014) 7461–7466, https://doi.org/10.1002/adfm.201402519.
[41] J. Guo, P. Pang, Q. Cai, Effect of trace residual ionic impurities on the response of chemiresistor sensors with dithiol-linked monolayer-protected gold (nano)clusters as sensing interfaces, Sens. Actuators B: Chem. 120 (2007) 521–528, https://doi.org/10.1016/j.snb.2006.03.014.
[42] C.A. Neugebauer, M.B. Webb, Electrical conduction mechanism in ultrathin, evaporated metal films, J. Appl. Phys. 33 (1962) 74–82, https://doi.org/10.1063/1.1728531.
[43] R.H. Terrill, T.A. Postlethwaite, C. Chen, C. Poon, An Terzis, A. Chen, et al., Monolayers in three dimensions: NMR, SAXS, thermal, and electron hopping studies of alkanethiol stabilized gold clusters, J. Am. Chem. Soc. 117 (1995) 12537–12548, https://doi.org/10.1021/ja00155a017.
[44] N.R. Bhakta, P.G. Woodruff, Human asthma phenotypes: from the clinic, to cytokines, and back again, Immunol. Rev. 242 (2011) 220–232, https://doi.org/10.1111/j.1600-065x.2011.01032.x.
[45] E.D. Bateman, S.S. Hurd, P.J. Barnes, J. Bousquet, J.M. Drazen, J.M. FitzGerald, et al., Global strategy for asthma management and prevention: GINA executive summary, Eur. Respir. J. 31 (2008) 143–178, https://doi.org/10.1016/j.arbres.2021.10.003.
[46] K. Cowan, T.W. Guilbert, Pediatric asthma phenotypes, Curr. Opin. Pediatr. 24 (2012) 344–351, https://doi.org/10.1097/MOP.0b013e32835357ab.
[47] J. Zhang, X. Wang, Y. Chen, W. Yao, Correlation between levels of exhaled hydrogen sulfide and airway inflammatory phenotype in patients with chronic persistent asthma, Respirology 19 (2014) 1165–1169, https://doi.org/10.1111/resp.12372.
[48] J.M. Spergel, M.I. Fogg, A. Bokszczanin-Knosala, Correlation of exhaled nitric oxide, spirometry and asthma symptoms, J. Asthma 42 (2005) 879–883, https://doi.org/10.1080/02770900500371344.

Xuemei Liu is currently a Ph.D. candidate at Institute of Analytical Chemistry, Department of Chemistry, Zhejiang University, Hangzhou, under the supervision of Prof. Jianmin Wu. Her research interests include artificial olfactory gas sensors and its potential application in disease diagnosis.

Zehui He is currently a Master degree candidate at Institute of Analytical Chemistry, Department of Chemistry, Zhejiang University, Hangzhou, under the supervision of Prof. Jianmin Wu. His research interests include research on artificial olfactory sensor materials.

Shiyuan Xu is currently a Ph.D. candidate at Institute of Analytical Chemistry, Department of Chemistry, Zhejiang University, Hangzhou, under the supervision of Prof. Jianmin Wu. Her research interests include gas sensing arrays and its potential application in clinical diagnosis.

Jianmin Wu is currently a professor at Institute of Analytical Chemistry, Department of Chemistry, Zhejiang University, Hangzhou. He received his Master's degree of Analytical Chemistry and Doctor's degree of Environment Science from Zhejiang University. He was invited to be a visiting scholar of University of California, San Diego (UCSD). His research focuses on artificial olfactory chemical sensor, biomaterials clinical mass spectrometry. The application of these research fields has expanded to clinical diagnosis via exhale breath, liquid biopsy and tissue biopsy, as well as theranostics for healthcare monitoring.

Jiaying Wu is currently a graduate student at Institute of Analytical Chemistry, Department of Chemistry, Zhejiang University, Hangzhou, under the supervision of Prof. Jianmin Wu. Her researches focus on the improvement of gas sensors based on graphene materials.